ISSN 2706-655X Vol. 7, Issue 3: 93-100, DOI: 10.25236/IJFET.2025.070313

# Three-Dimensional Numerical Study on the Flow Characteristics of Circular Cylinder Considering the Influence of Free-End

**Jin Miao[a], Hongyuan Sun[b,*], Dexin Liu[c]**

*School of Naval Architecture and Port Engineering, Shandong Jiaotong University, Weihai, Shandong Province, 264209, China*
*[a]15589425509@163.com, [b]hongyuan_000@163.com, [c]liu516016362@163.com*
**Corresponding author*

***Abstract:*** *Most floating offshore platforms are cylindrical with low aspect ratios, whereas most existing research focuses on structures with high aspect ratios. Research on the influence of the free-end effect on the flow around a cylinder at low aspect ratios is still insufficient. Therefore, in this study, the computational fluid dynamics (CFD) method was used to numerically simulate the flow characteristics of finite and infinite cylinders at different flow rates, and the influence of the free-end effect on the flow characteristics of the cylinders was discussed. The results show that the free-end effect significantly interferes with the flow characteristics of finite cylinders. In particular, for a shorter cylinder (L/D = 2), the free-end effect caused obvious vortex separation and flow instability, resulting in a higher vortex intensity. With an increase in flow velocity, the influence of the free-end effect weakened; however, the flow remained unstable. In contrast, the flow of an infinite cylinder is not affected by the free-end effect and always maintains a stable flow. The vortex region was small, and with the increase in flow velocity, the flow gradually tended to be inertia-dominant, showing more stable flow characteristics.*

***Keywords:*** *Flow Around Circular Cylinder; Free-End; CFD; Aspect Ratio; SST k-ω*

## 1. Introduction

A finite-length cylinder is an important bluff body structure that is commonly used in marine engineering. Typical examples include floating offshore platforms (such as Spar and Monocolumn platforms)[1]. Many factors affect the flow around a finite cylinder, among which the aspect ratio and Reynolds number Re play the most critical roles[2]. Therefore, it is of great practical significance to study the flow around a finite-length cylinder at different aspect ratios and inflow velocities.

The problem of flow around a finite cylinder has been studied extensively. The experimental data of Eisenlohr and Eckelmann[3] show that the discontinuity observed at $Re \approx 90$ is a three-dimensional effect. They also described the basic pressure and velocity distribution of the wake near the stern. Park et al.[4] used particle image velocimetry (PIV), and a finite-length cylinder with a Reynolds number *of* $Re = 7.5 \times 10^3$ was simulated using this technique. Through analysis, it is found that the free end of the tip vortex appears in pairs, and after analysis, it is found that the tip vortex appears in pairs. The tip vortex is caused by the downwash flow of the end face and the flow around the cylinder. An interaction is generated. Akilli and Rockwell[5] studied a finite-length inverted cylinder in water with aspect ratios of 1 and 2 using particle image velocimetry, and their results showed the formation process of large-scale vortices.

With the development of computational fluid dynamics (CFD) technology, numerical simulations have become a key method for studying flow around cylinders. Zdravkovich et al.[6] measured the resistance of the free-end cylinder under the condition that the Reynolds number $Re$ is $6\times10^4$ to $2.6\times10^7$ and the length-diameter ratio $L/D$ is 1 to 10. The results show that when $L/D \leq 3$, the low-pressure region near the free end gradually disappears, forming an asymmetric flow pattern. Based on the immersed boundary method, Palau-Salvador et al.[7] used large eddy simulation to simulate the flow around two finite-length cylinders ($L/D$ = 2.5,5) at two Reynolds numbers ($Re = 4.3 \times 10^4$, $2.2 \times 10^4$) working condition. Experimental and simulation analyses were performed. The results showed that the alternating vortex shedding of the shorter cylinder occurred only near the wall and was unstable. Liu et al.[8] used LES to study the flow around a finite cylinder under high $Re$ conditions, analyzed the variation of drag coefficient when $L/D$ = 45-100, and discussed the influence of end effect on drag characteristics and

ISSN 2706-655X Vol. 7, Issue 3: 93-100, DOI: 10.25236/IJFET.2025.070313

velocity field distribution.

In this study, a computational fluid dynamics (CFD) numerical simulation method was used to compare a finite-length cylinder with a finite-length cylinder with a high ratio of 2 and 5. The mean resistance, three-dimensional streamline diagram, two-dimensional streamline diagram at different sections, and three-dimensional instantaneous vorticity cloud diagram were analyzed, and the influence of the free-end effect on the flow around the cylinder was analyzed in detail.

## 2. Numerical model

### *2.1 Governing Equations*

For three-dimensional unsteady incompressible viscous flow, the continuity and momentum equations are as follows:

$$\frac{\partial \mathrm{u}_i}{\partial x_i} = 0 \tag{1}$$

$$\frac{\partial \mathrm{u}_i}{\partial t} + \frac{\partial}{\partial x_j}(u_i u_j) = -\frac{1}{p}\frac{\partial p}{\partial x_i} + \frac{\partial}{\partial x_j}(v\frac{\partial u_i}{\partial x_j}) + f_i \tag{2}$$

Where $u_i$ and $u_j$ are the velocity components, $p$ is the pressure, *and* $v$ is the total viscosity coefficient expressed as a laminar viscosity system. The sum of the number and turbulent viscosity coefficient, where the turbulent viscosity coefficient is obtained by the turbulence model, and $f_i$ is the external force component.

The SST k-ω model used in the numerical simulation in this study was a Reynolds-averaged method. The SST k-ω model had a good effect on both the near-wall and far-field calculations. Compared with the standard k-ω model, the SST k-ω model considers the shear stress transport mode, changes the turbulence constant in the model, and performs better in solving the negative pressure gradient in the turbulence problems. These characteristics render the SST k-ω model suitable for a wide range of applications.

SST k-ω model transport equation

$$\frac{\partial}{\partial t}(\rho k) + \frac{\partial}{\partial x_i}(\rho k u_i) = \frac{\partial}{\partial x_j}\left(\Gamma_k \frac{\partial k}{\partial x_j}\right) + \widetilde{G}_k - Y_k + S_k \tag{3}$$

$$\frac{\partial}{\partial t}(\rho \omega) + \frac{\partial}{\partial x_i}(\rho \omega u_i) = \frac{\partial}{\partial x_j}\left(\Gamma_\omega \frac{\partial \omega}{\partial x_j}\right) + G_\omega - D_\omega + S_\omega \tag{4}$$

Where, $i, j \in (1,2,3)$, $\Gamma_k = \mu + u_i / \sigma_k$ and $\Gamma_\omega = \mu + u_i / \sigma_\omega$ are the effective diffusion terms of $k$ and $\omega$, $\sigma_k$ and $\sigma_\omega$ are the corresponding Prandtl numbers, and $\mu$ is the molecular viscosity of the fluid. $\widetilde{G}_k$ are the production terms of turbulence kinetic energy $k$, $G_\omega$ is the production term of $\omega$, $Y_k$ is the dissipation term of $k$, $Y_\omega$ is the dissipation term of $\omega$, $D_\omega$ is the cross diffusion term; $S_k$ and $S_\omega$ are the user-defined source terms. $\Gamma_k$ and $\Gamma_\omega$ expressed as:

$$\Gamma_k = \mu + \frac{\mu_t}{\sigma_k} \tag{5}$$

$$\Gamma_\omega = \mu + \frac{\mu_t}{\sigma_\omega} \tag{6}$$

### *2.2 Mesh Generation and Solution Method*

#### *2.2.1 Computational Domain and Mesh Generation*

In this study, finite-and infinite-length cylinder models were selected for the calculations and analyses.

ISSN 2706-655X Vol. 7, Issue 3: 93-100, DOI: 10.25236/IJFET.2025.070313

The cylinder diameter $D$ was 0.1m, and the overall calculation domain size was $40D \times 20D \times ZD$. As shown in figure 1. The left side of the model was set as the velocity inlet, which was $10D$ away from the center of the cylinder, and the right side was set as the pressure outlet, which was $30D$ from the center of the cylinder. The upper and lower boundaries were symmetrical, with a distance of $20D$, and the cylinder wall was a non-slip boundary, whereas the other was a symmetrical boundary. In the infinite cylinder, the spanwise height was $Z = 3D$, as shown in figure 2 (a). In the finite cylinder, the spanwise heights were $Z = 2D$ and $5D$, as shown in figure 2 (b).

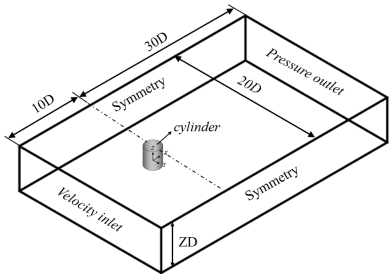


*Figure 1: Three-dimensional model of flow around a cylinder in the computational domain.*

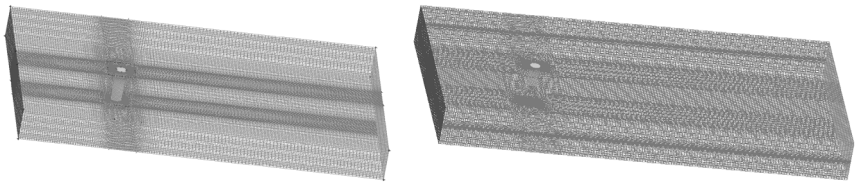

*(a)* *(b)*

*Figure 2: Schematic of finite and infinite cylindrical grid divisions.*

### *2.2.2 Solution Method*

In this study, the Reynolds-averaged Navier-Stokes (RANS) method was used to model the flow field for the incompressible three-dimensional turbulent flow around a cylinder to obtain the numerical solution of the steady-state average flow structure and main turbulence characteristics. To accurately capture the change in the boundary layer near the surface of the cylinder and the turbulent separation behavior in the wake region, the Shear Stress Transport (SST k-ω) turbulence model was selected. A numerical simulation was performed using ANSYS Fluent software. The steady-state solution strategy and SIMPLEC algorithm were used to address the coupling of speed and pressure to ensure the stability and convergence of the calculation. A second-order upwind scheme was used for spatial discretization to improve the calculation accuracy and enhance the analytical ability of the turbulence structure. Local grid refinement was performed in key flow areas to ensure the reliability and accuracy of the results.

## *2.3 Validation of the numerical methods*

### *2.3.1 Calculation Conditions*

In this study, finite long cylinders and infinite long cylinders were investigated using numerical simulations. In the simulation of a finite cylinder, two different aspect ratios ($L/D = 2$ and $L/D = 5$) were selected, and the influence of the free-end effect on the flow characteristics was analyzed. To comprehensively evaluate the flow characteristics under different working conditions, this study set the flow velocity range from 0 m/s to 0.65 m/s, and the cylinder diameter was set to 0.1 m. By comparing the flow characteristics of finite-and infinite-length cylinders under the same incoming flow conditions, the influence of the free-end effect on the flow field of the cylinder was discussed in depth.

### *2.3.2 Numerical simulation verification*

To verify the accuracy and stability of the numerical simulation results, this study selected three different grids for grid independence verification, selected the flow rate $U = 0.2$ m/s, $Re = 20000$ as an example, and compared the simulation results with those of Bai [9] under the same working conditions. The grid independence test is a key step to verify whether the grid division is fine enough, whether it can reflect the accurate calculation results, and avoid the calculation error caused by a grid that is too coarse. Table 1 lists the relevant calculation results for the three grids, including the number of grids, $Cl$ amplitude, $Cd$ mean, and $St$ number for each grid.

ISSN 2706-655X Vol. 7, Issue 3: 93-100, DOI: 10.25236/IJFET.2025.070313

*Table 1: Mesh simulation results.*

| Mesh | A | B | C | Bai[9] |
|---|---|---|---|---|
| Number of units | 322249 | 410928 | 509679 | ---- |
| $C_{l,rms}$ | 0.65 | 0.75 | 0.78 | 0.71 |
| $C_{d,mean}$ | 1.14 | 1.19 | 1.23 | 1.17 |
| *St* | 0.230 | 0.235 | 0.246 | 0.210 |

In the grid independence test, by comparing the calculation results of different grids, we found that grid B showed good stability in the numerical changes of *the Cl* range, *Cd* mean, and *St* number. This is similar to the results of Bai. Simultaneously, Grid B has fewer calculations than Grid C, which can effectively reduce the calculation time and resource consumption while ensuring sufficient accuracy. Considering the calculation accuracy, efficiency, and consistency with the results of existing literature, Grid B was selected as the final calculation grid for this study.

### *2.3.3 Numerical simulation verification*

After grid independence verification, the M2 grid was selected in this study to ensure the accuracy of the numerical model, and the numerical simulation data of Zhang [10] were compared and verified. The flow velocity *U* was 0-0.6 m/s, and the mean drag and lift standard deviations were compared and analyzed. As shown in figure 3, 'Present simulation' represents the numerical simulation results of this study, and 'Zhang present' represents the numerical simulation results of Zhang.

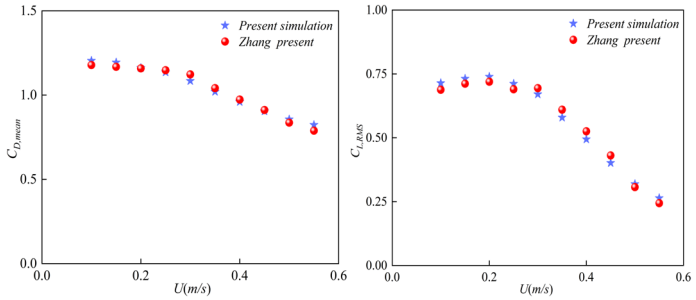


*Figure 3: Numerical comparison and verification of the mean lift and drag of the cylinder at different reduced velocities.*

It can be seen from the diagram that the current numerical simulation results are in good agreement with the simulation results of Zhang under different flow velocity conditions. Both the *Cd* (figure. 3a) and *Cl* (figure. 3b) values show similar changes: as the flow rate increases, the values gradually decrease, and the magnitude of change tends to decrease. Although there is a certain deviation under low flow rate conditions, the overall trend is highly consistent, indicating that the current numerical simulation results are highly reliable, thus verifying the accuracy of the numerical simulation method used in this study.

## 3. Results and discussion

### *3.1 Resistance coefficient analysis*

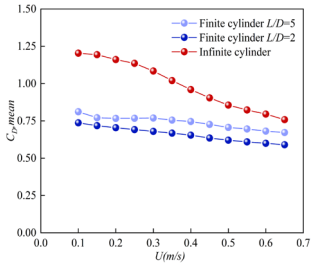


*Figure 4: Variation in mean drag of finite and infinite cylinders with incoming flow velocity.*

Figure 4 shows the resistance mean value diagram of the finite and infinite cylinders with respect to the change in flow velocity. In the diagram, with an increase in flow velocity, the resistance coefficient of the finite cylinder decreases gradually with an increase in flow velocity. Simultaneously, at the same flow velocity, the resistance coefficient of the finite cylinder with $L/D = 2$ was smaller, and the resistance

ISSN 2706-655X Vol. 7, Issue 3: 93-100, DOI: 10.25236/IJFET.2025.070313

coefficient of the finite cylinder with $L/D$ = 5 was larger. This indicates that the cylinder with a smaller ($L/D$ = 2) exhibits a lower drag coefficient in the flow, which is in sharp contrast to the cylinder with a larger aspect ratio ($L/D$ = 5) and higher drag coefficient. For a short finite cylinder ($L/D$ = 2), owing to the significant free-end effect, flow interference, and vortex generation at the free end, strong flow separation occurs, thus reducing the stability of the flow and affecting the drag coefficient. Although the free-end effect is stronger in short cylinders, its effect on the flow may decrease the local resistance, particularly at lower flow rates. As the flow rate increased, the vortex and flow separation effects gradually stabilized, resulting in a decrease in the resistance coefficient.

For a long finite cylinder ($L/D$ = 5), the free-end effect was relatively weak, the flow tended to be stable, the vortex intensity generated by the fluid flow around it was small, and the flow became more stable. However, owing to the increase in the length of the cylinder, the flow characteristics were more complex, and the drag coefficient was larger.

### *3.2 Lift resistance time history curve*

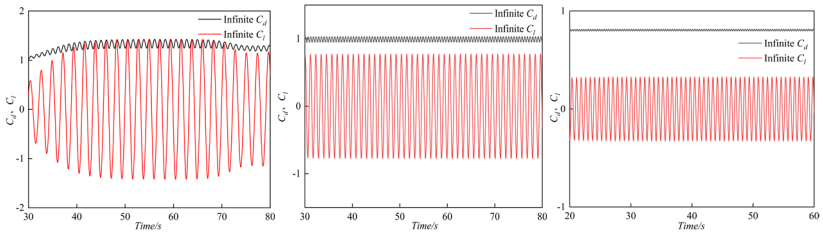


*U=0.2* *U=0.4* *U=0.6*

*Figure 5: Lift-drag curves of an infinite cylinder at various inflow velocities.*

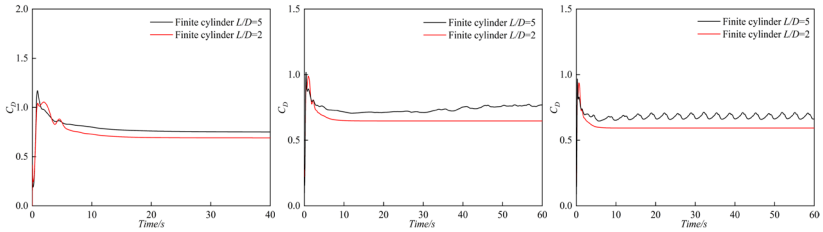


*U=0.2* *U=0.4* *U=0.6*

*Figure 6: Resistance curves of a finite cylinder for different inflow velocities.*

Figure 5 and 6 show the variations in the lift and drag coefficients of the infinite and finite cylinders with time at different flow rates. The drag coefficient of the infinite cylinder gradually tended to stabilize with an increase in the flow velocity, showing a small fluctuation range, indicating that the flow around the infinite cylinder was mainly dominated by the inertial force, and the flow gradually stabilized. However, the finite cylinder exhibited a significant free-end effect, particularly at a low flow rate ($U$ = 0.2 m/s), and the drag coefficient of the cylinder with $L/D$ = 2 fluctuated significantly. As the flow rate increased, the fluctuation gradually decreased, but the drag coefficient remained elevated. In contrast, the flow of the cylinder with $L/D$ = 5 was relatively stable owing to the weak free-end effect, and the fluctuation of the drag coefficient was small. Overall, a smaller $L/D$ ratio showed a more significant free-end effect, resulting in larger resistance fluctuations, whereas a cylinder with a larger aspect ratio showed more stable flow characteristics. These results further verify the influence of the free-end effect on the flow around a finite-length cylinder and emphasize the significant effect of the aspect ratio on flow stability.

### *3.3 Characteristics of vortex field*

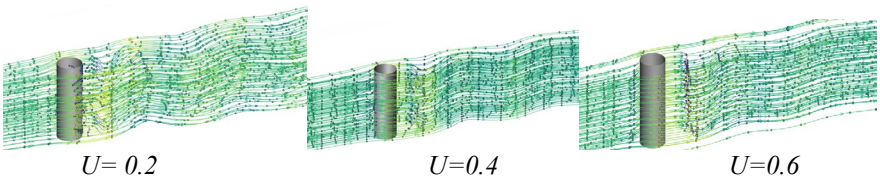

*U= 0.2* *U=0.4* *U=0.6*

*Figure 7: Three-dimensional streamlines of an infinite cylinder at various inflow velocities.*

ISSN 2706-655X Vol. 7, Issue 3: 93-100, DOI: 10.25236/IJFET.2025.070313

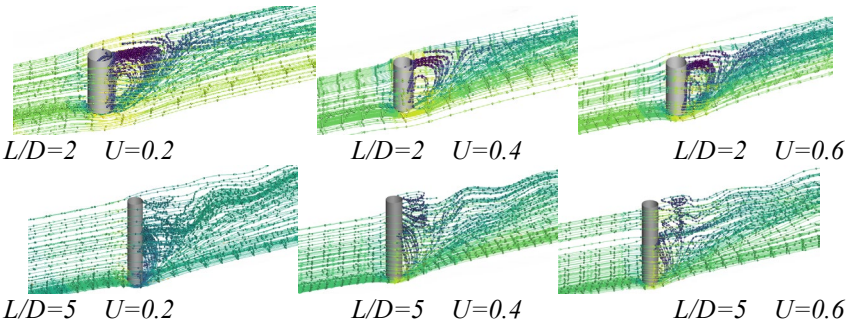


*Figure 8: Three-dimensional streamlines of a finite cylinder at various inflow velocities.*

From the three-dimensional streamlines in Figure 7 and 8, we can further analyze the flow characteristics of the finite and infinite cylinders at different flow rates and the influence of the free-end effect. The streamline distribution of the infinite cylinder at different flow rates remained symmetrical and stable, and the flow was mainly dominated by inertial force. Even at a higher flow rate ($U = 0.6$ m/s), the generation of eddy currents and curvature of the streamline were relatively small, indicating that the flow process of the fluid was stable and not significantly affected by the free end. This stability is a significant feature of infinitely long cylinder.

In contrast, a finite-length cylinder exhibits complex flow behavior. When the flow velocity is low ($U = 0.2$ m/s), on the cylinder with $L/D = 2$, the fluid forms strong eddy currents and flow separation in the free-end region, and the streamline appears more disordered, reflecting the influence of the free-end effect on the flow. This free-end effect is particularly evident in short cylinders ($L/D = 2$). The vortex intensity was large, flow instability was significantly increased, and the drag coefficient was relatively high for this configuration. With the increase in flow velocity ($U = 0.4$ m/s and $U = 0.6$ m/s), although the vortex region tended to shrink and the flow became relatively stable, the influence of the free-end effect still existed, which was manifested by the bending of the streamline and the existence of the vortex in the free-end region. When the aspect ratio increases to $L/D = 5$, the free-end effect gradually weakens, and the stability of the fluid flow around it improves. The streamline diagram shows that the flow of the cylinder with $L/D = 5$ becomes more stable at different flow rates, the eddy current region shrinks, and the streamline tends to be regular. Nevertheless, the longer cylinder is still affected by the free-end effect to a certain extent; however, compared with the cylinder with $L/D = 2$, the degree of influence is significantly reduced, and flow stability is enhanced.

### *3.4 Streamline diagrams of different cross sections of cylinder*

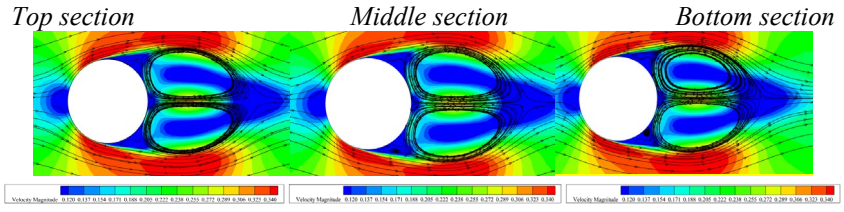


*Figure 9: Streamlines of different cross sections of an infinite cylinder.*

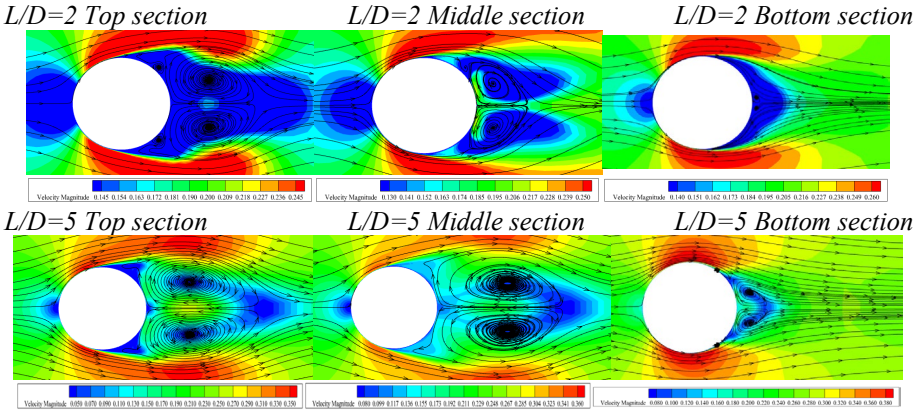


*Figure 10: Streamline diagrams of different cross-sections of a finite-length cylinder.*

ISSN 2706-655X Vol. 7, Issue 3: 93-100, DOI: 10.25236/IJFET.2025.070313

The streamlines of different sections in Figure 9 and 10 show that the free-end effect significantly affects the flow characteristics of the finite and infinite cylinders. For an infinite cylinder, the streamline distribution in different sections is symmetrical and stable. In particular, when $L/D$ = 5, the flow around the fluid showed a stable flow characteristic, the streamline distribution was uniform, and the vortex region was small, indicating that the flow was mainly affected by the inertial force, and the flow stability had no obvious free-end effect. In the finite-length cylinder, especially the cylinder with $L/D$ = 2, the streamline showed an obvious offset and bending at the free end, the vortex region was more significant, and the vortex intensity at the free end was larger, showing a strong free-end effect on the flow interference. In a finite cylinder with $L/D$ = 5, although the free-end effect was weakened, vortex and flow separations near the free end were still observed, which further verified the inhibition of the aspect ratio on the free-end effect. In general, a smaller aspect ratio ($L/D$ = 2) leads to a more significant free-end effect and an increase in flow instability, whereas a larger aspect ratio ($L/D$ = 5) stabilizes the flow, and the eddy current region and flow interference are reduced.

### *3.5 Three-dimensional vorticity cloud*

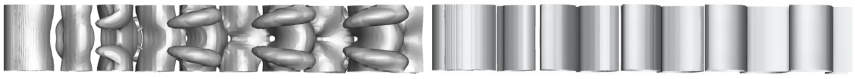

*Ur=0.2* *Ur=0.6*

*Figure 11: Three-dimensional vorticity cloud of an infinite cylinder at different inflow velocities.*

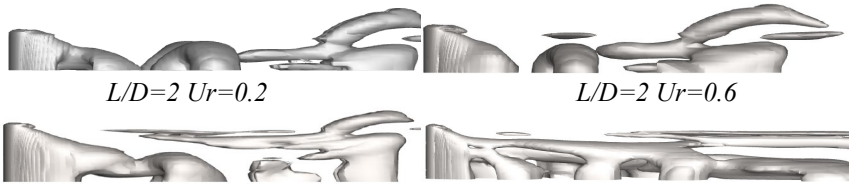

*L/D=2 Ur=0.2* *L/D=2 Ur=0.6*

*L/D=5 Ur=0.2* *L/D=5 Ur=0.6*

*Figure 12: Three-dimensional vorticity cloud of a finite cylinder at different incoming-flow velocities.*

The three-dimensional vorticity contours in Figure 11 and 12 clearly show that the free-end effect significantly affects the flow characteristics of the finite and infinite cylinders. In the vorticity cloud map of an infinitely long cylinder, with an increase in flow velocity ($U$ = 0.2 m/s to $U$ = 0.6 m/s), the distribution of vorticity gradually became more compact and symmetrical, and the flow was more stable. The vortex was mainly concentrated at the rear of the cylinder, and the vorticity was more uniform at low flow velocities. As the flow velocity increased, the vortex area decreased, indicating that the flow tended to be inertially dominated and stable. For the finite length cylinder, especially in the cylinder with $L/D$ = 2, the vorticity cloud diagram shows an obvious vortex separation and vorticity accumulation in the free-end region. In particular, at a low flow velocity ($U$ = 0.2 m/s), the vorticity intensity at the free end was high, the vortex area was wide, and the flow was unstable. With an increase in flow velocity, although the vortex distribution is improved and the vorticity region becomes more concentrated, the influence of the free end still exists, and the vorticity distribution is not as regular as that of an infinite cylinder. For a long finite cylinder ($L/D$ = 5), the free-end effect was weakened, the vorticity distribution became relatively stable, the flow tended to be stable, and the intensity of the vortex was weakened. Therefore, the aspect ratio is low.

## 4. Summary

In this study, the flow characteristics of finite and infinite cylinders were compared and studied using the CFD numerical method. The mean resistance, three-dimensional streamline distribution, streamline characteristics of each section, and three-dimensional instantaneous vorticity distribution of the cylinder at different inflow velocities were analyzed. The influence of the free-end effect on the flow characteristics of the cylinder was discussed in detail. The following conclusions were drawn:

(1) The interference of the free-end effect on the flow around a finite-length cylinder: The free-end effect significantly affects the flow characteristics around finite-length cylinders. In particular, for the shorter cylinder ($L/D$ = 2), the free-end effect led to strong flow interference, characterized by obvious vortex separation and asymmetric streamline distribution. At low flow velocities, the vortex region was larger, the flow was unstable, and the vorticity intensity was higher, which increased the flow resistance

ISSN 2706-655X Vol. 7, Issue 3: 93-100, DOI: 10.25236/IJFET.2025.070313

and instability. As the flow rate increased, the influence of the free-end effect weakened; however, vortex and flow separation still existed, and flow stability was not fully restored.

(2) Infinite cylinder without free-end effect: The flow around the infinite cylinder is unaffected by the free-end effect, showing stable flow characteristics. The streamline and vorticity cloud diagrams show that the infinite cylinder maintains a symmetrical and stable flow at different flow rates, the vortex region is small, and the flow is almost unaffected by free-end interference. With an increase in flow velocity, the flow tended to be dominated by inertia, the vortex area was reduced, the flow was more stable, and the drag coefficient gradually decreased.

## References

*[1] MA Y, CHEN C, FAN T, et al. Research on motion inhibition method using an innovative type of mooring system for spar floating offshore wind turbine[J]. Ocean Engineering, 2021, 223:108644.*
*[2] QIU T, LIN W, DU X, et al. Mass ratio effect on vortex-induced vibration for two tandem square cylinders at a low Reynolds number[J]. Physics of Fluids, 2021, 33:123604.*
*[3] Holger E, Helmut E, et al. Flow around finite lengthed cylinders at low Reynolds number: End effects and their origins. Physics of Separated Flows- Numerical, Experimental, and Theoretical Aspects 1993, 40, 208-215.*
*[4] PARK C W, LEE S J, et al. Effects of free-end corner shape on flow structure around a finite cylinder[J]. Journal of Fluids and Structures, 2004, 19(2): 141-158.*
*[5] Akilli H, Rockwell D, et al. Vortex formation from a circular cylinder in shallow water[J]. Physics of Fluids, 2002, 14, 2957-2967.*
*[6] Zdravkovich M M, Brand V P, Mathew G et al. Flow past short circular cylinders with two free ends[J]. Journal of fluid mechanics. 2006, 203,557-575.*
*[7] D PALAU-SALVADOR G, STOESSER T, FRÖHLICHJ, et al. Large eddy simulations and experiments of flow around finite-height cylinders[J]. Flow, Turbulence and Combustion, 2010, 84 (2):239-275.*
*[8] Liu, X.Y.; Zhao, M.; Liu, M.Y. Study of end-face effects on flow around finite circular cylinder at high Reynolds number[J]. Journal of fluid mechanics. 2019, 38, 362-369.*
*[9] Bai Z.Y.; Study on the dynamic response characteristics of a deep-water semi-submersible platform under slamming motion[D]. Shanghai Jiao Tong University, 2013.*
*[10] J. Zhang, Research on vortex-induced motion characteristics of foundation structure of Spar floating wind turbine[D]. ShanDong JiaoTong University, 2022.*